In vitro antimicrobial effects and mechanism of atmospheric-pressure He/O$_2$ plasma jet on *Staphylococcus aureus* biofilm

In vitro antimicrobial effects and mechanism of atmospheric-pressure He/O$_2$ plasma jet on *Staphylococcus aureus* biofilm

Zimu Xu[1], Jie Shen[2], Cheng Cheng[2,3], Shuheng Hu[1], Yan Lan[2] and Paul K Chu[4]

[1] School of Resources and Environmental Engineering, Hefei University of Technology, Hefei, Anhui Province 230009, People's Republic of China
[2] Institute of Plasma Physics, Chinese Academy of Sciences, PO Box 1126, Hefei 230031, People's Republic of China
[3] Center of Medical Physics and Technology, Hefei Institutes of Physical Science, Chinese Academy of Sciences, Hefei 230031, People's Republic of China
[4] Department of Physics and Materials Science, City University of Hong Kong, Tat Chee Avenue, Kowloon, Hong Kong, People's Republic of China

E-mail: chengcheng@ipp.ac.cn (C Cheng), shuheng.hu@163.com (S Hu) and paul.chu@cityu.edu.hk (P Chu)

Abstract

The antimicrobial effects and associated mechanism of inactivation of *Staphylococcus aureus* (*S. aureus*) NCTC-8325 biofilms induced by a He/O$_2$ atmospheric-pressure plasma jet (APPJ) are investigated *in vitro*. According to CFU (colony forming units) counting and the resazurin-based assay, the 10 min He/O$_2$ (0.5%) APPJ treatment produces the optimal inactivation efficacy (>5 log10 ml^{-1}) against the *S. aureus* biofilm and 5% of the bacteria enter a viable but non-culturable (VBNC) state. Meanwhile, 94% of the bacteria suffer from membrane damage according to SYTO 9/PI counterstaining. Scanning electron microscopy (SEM) reveals that plasma exposure erodes the extracellular polymeric substances (EPS) and then the cellular structure. The H$_2$DCFDA-stained biofilms show larger concentrations of intracellular reactive oxygen species (ROS) in membrane-intact bacteria with increasing plasma dose. The admixture of oxygen in the working gas highly contributes to the deactivation efficacy of the APPJ against *S. aureus* and the plasma-induced endogenous ROS may work together with the discharge-generated ROS to continuously damage the bacterial membrane structure leading to deactivation of the biofilm microbes.

Keywords: atmospheric-pressure plasma jet (APPJ), *Staphylococcus aureus*, biofilm inactivation, reactive oxygen species (ROS)

(Some figures may appear in colour only in the online journal)

1. Introduction

Many types of planktonic bacteria can attach to each other to form dynamic biofilms on different surfaces and materials. In the presence of extracellular polymeric substances (EPS) such as water, polysaccharides, DNA, and lysed bacteria debris, the microbial biofilms can offer bacteria enhanced protection and nutrition traps. Biofilm bacteria are different from their planktonic counterparts in terms of the physiology and environmental stress resistance based on EPS protection and the cell-to-cell quorum sensing (QS) system, which regulates the interbacterial communication, conjugation, and coordination [1, 2]. Therefore, the host immune system and antibiotics are less effective in deactivating microbial biofilms, leading to high health cost, morbidity, and mortality in the treatment of biofilm-related hospital acquired infections (HAI), implant
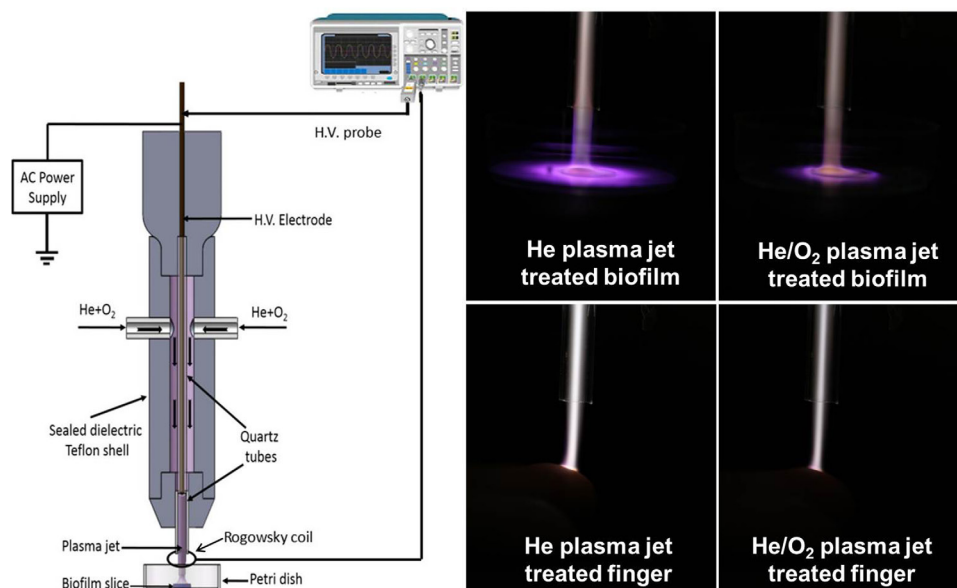
J. Phys. D: Appl. Phys. **50** (2017) 105201

Z Xu *et al*

Figure 1. Diagram and electrical schematic of the APPJ device and typical photographs of the He and He/O$_2$ APPJ.

infection, and chronic wounds [3]. Hence, new approaches with better biofilm-controlling effects are needed.

A cold atmospheric-pressure plasma is a useful sterilizing tool to treat biofilm-contaminated human skin, canal roots, as well as biomedical devices [4–19]. In particular, the atmospheric-pressure plasma jet (APPJ) is effective in deactivating various kinds of Gram-positive and negative microbial biofilms and possesses many advantages such as high inactivation efficiency, no toxic residues, and low treatment costs [20–29]. The antimicrobial efficacy of APPJ on *C. albicans*, *S. mutans*, and human saliva biofilms were investigated *in vitro* by Koban *et al* [30, 31] and the APPJ could be a substitute for chemical antiseptics in eradicating biofilms. The APPJ penetration depth into *P. gingivalis* and *E. faecalis* biofilms determined by Xiong *et al* [32] and Pei *et al* [33] was about 15 μm and 25.5 μm, respectively. Sysoliatina *et al* [34] found that an exposure time of 4 min was adequate in killing 9 log10 CFU (colony forming unit) of biofilm *S. epidermidis* with an Ar-Air APPJ. Vandervoort *et al* [35] and Zelaya *et al* [36] studied the anti-microbial capacity of a 13.56 MHz RF-driven He/N$_2$ APPJ against *P. aeruginosa* biofilms with different N$_2$ ratios and 7 log10 CFU reduction (reduction of 10^7 bacteria CFUs) was observed after minutes. Moreover, the antimicrobial effects on *S. aureus* biofilms by APPJs for different gas compositions and treatment doses have been explored. CFU reduction of 5.5 log10 ml^{-1} was by He/O$_2$ APPJ treatment *in vitro* for 2 min by Alkawareek *et al* [22] and 6.7 log 10 ml^{-1} after 6 min by Flynn *et al* [37]. Matthes *et al* [25] found that an RF-driven Ar APPJ produced considerable antimicrobial effects on *S. aureus* ATCC-6538 biofilms and the plasma dose played a crucial role. Delben *et al* [23] investigated the inactivation efficacy of a DC-driven Ar APPJ against *S. aureus* biofilms and *C. albicans/S. aureus* dual-species biofilms. Considerable deactivation effects were observed from *S. aureus* under two conditions corresponding to 2 log10 CFU ml^{-1} and 1.2 log10 CFU ml^{-1} reduction, respectively, after exposure for 1 min.

APPJ possesses the characteristics of transient and thermal non-equilibrium and highly reactive chemistry so that charged species can be transported rapidly and efficiently [38–41]. APPJ produces reactive oxygen species (ROS) such as $\cdot O_2^-$, $^1O_2$, $\cdot OH$, and O_3 [42] while emitting UV (ultra-violet) radiation [43] and electric fields [44] simultaneously. These environmental stresses can potentially trigger cell degradation by damaging bio-macromolecules such as proteins, lipids, and DNAs, thereby affecting the cellular metabolism, electron transportation, intracellular electric fields generation, and intracellular ROS production [43–50]. Our previous work indicated that helium APPJ could induce significant oxidative stress in biofilm bacteria and trigger intracellular production of ROS. The plasma-generated reactive species and plasma-induced endogenous ROS possibly contributed to bacteria death synergistically [51].

A mixture of O$_2$ with noble gases or nitrogen can enhance the inactivation efficacy of plasmas against microorganisms in both planktonic and biofilm bacteria by damaging the cellular structure and functions due to more plasma-generated ROS [52–55]. However, the specific ROS-driven intracellular interactions and related mechanism on final deactivation are still not well understood. Furthermore, the relationship between discharge-generated ROS and plasma-induced endogenous ROS in bacteria is not clear. In this work, the role of O$_2$ in the helium discharge against *S. aureus* biofilms is investigated systematically *in vitro*.

2. Materials and methods

2.1. Plasma source

Figure 1 shows the diagram and the electrical schematic for the AC-driven APPJ source used in this study as previously described by Xu *et al* [51]. A copper rod was fixed at the center of a thin quartz tube with one side sealed to serve as a single electrode. The tube was wrapped with a Teflon shell tightly

and connected to the quartz nozzle tube. A mixture containing helium (99.995%) and oxygen was the working gas and the flow rate was 6.7 standard liters per minute (SLM). The electrical characteristics of the APPJ was monitored by a high-voltage probe (P6015A) and Rogowsky coil with a digital oscilloscope (Tektronix MSO 5104) (figure 1). The input voltage was 20 kV for the He APPJ and periodical discharge occurred at a frequency of 38 kHz. The average plasma power was calculated by the following formula:

$$P = \frac{1}{T} \int_0^T u(t) i(t) \mathrm{d}t,$$

where T is the discharge period and the average discharge power is about 14 W. The plasma power was kept at this value during the experiments. The photographs of the He and He/O$_2$ APPJ treated biofilm slices and human skin are displayed in figure 1 which shows reduced coverage for the He/O$_2$ plasma compared to the helium discharge.

2.2. Preparation for S. aureus biofilms

Gram-positive bacterium *S. aureus* biofilms can form on human skins, biomaterials, and biomedical devices leading to infection [56]. In our experiments, the *S. aureus* strain NCTC-8325 with significant biofilm-forming capacity was cultured overnight, diluted to $1–2 \times 10^7$ CFU ml^{-1} in the TSBG (tryptic soy broth with 0.5% glucose) medium, and cultivated on a borosilicate slice (diameter = 8 mm, area $\approx$ 0.5 cm^2) for 12 h at 37 °C. For the CLSM (confocal laser scanning microscopy) examination, the biofilms were cultured on microwell dishes (Part No. P35G-1.5.20-C, MatTek Co., Ashland, MA, USA). The average thickness of the cultured *S. aureus* biofilms was 16.4 ± 2.0 μm as determined by fluorescence staining. After incubation, the medium was removed and the biofilms were rinsed gently by PBS (phosphate buffer saline) to remove planktonic and loosely attached bacteria. Prior to plasma exposure, the biofilms were kept at 37 °C in an incubator for 15 min for drying and water residues were hardly discernable on the biofilms afterwards.

2.3. Plasma exposure

The distance between the *S. aureus* biofilms and plasma jet nozzle was 10 mm in order for the plasma to cover the entire biofilm area. The exposure time was varied from 0 to 10 min and the biofilms treated with the gas mixture without discharge served as the control samples in order to eliminate the drying-triggered antimicrobial effects. To investigate the disinfection effects of the APPJ-generated UV, the plasma effluent was blocked by a sterile quartz plate but UV was allowed to reach the biofilms [57].

2.4. Deactivation effects on biofilm S. aureus by APPJ exposure

CFU counting and *D*-value (the decimal reduction time required to kill 90% of the organisms studied) calculation were used to study the cultivability of biofilm *S. aureus* after

plasma exposure. The *S. aureus* were dispersed from the biofilms ultrasonically for 20 min [26, 58] and re-suspended in 1 ml of PBS. Decimal dilutions were carried out before spreading on TSBG agar plates. The overnight culture was counted to assess the plasma-driven deactivation effect.

2.5. Optical emission spectroscopy (OES)

An AvaSpec-2048-8-RM spectrometer (gratings of 2400 grooves mm^{-1}) was employed to obtain the optical emission spectra of the He and He/O$_2$ APPJ. The optical fiber probe was installed 10 mm away from the plasma jet nozzle and instrumental broadening was about 0.11 nm determined by a mercury lamp.

2.6. Mass spectrometry (MS)

Mass spectrometry was conducted on the MBMS (molecular-beam mass spectrometer, Hiden EQP mass/energy analyzer HPR 60). The distance between the jet nozzle and orifice of MBMS was 10 mm and a time-averaged mode was implemented.

2.7. Cellular metabolic capacity of biofilm S. aureus

Resazurin (7-hydroxy-3H-phenoxazin-3-one 10-oxide) can diffuse into bacteria and be reduced to resorufin (7-Hydroxy-3H-phenoxazin-3-one) by intra-bacterial reductases and the non-reversible bio-chemical change of resazurin to fluorescent resorufin depends on the bacteria with metabolic ability [59]. Here, a resazurin-based toxicology assay kit (Sigma®, St. Louis, MO, USA) was utilized to monitor the bacterial metabolic ability of the biofilm *S. aureus* according to the manufacturer's instructions. The plasma-treated biofilms were re-suspended in PBS and resazurin was then added and cultured. A standard microplate reader (Varioskan Flash, Thermo-Fisher Scientific, US) was employed to measure the fluorescent intensity at excitation/emission (Ex/Em) wavelengths of 560/590 nm. The percentage of metabolic *S. aureus* after plasma exposure was calculated based on the control samples (set to 100%). The resazurin-added *d*H$_2$O (de-ionized water) without bacteria served as the control to determine the fluorescence background.

2.8. Membrane integrity of biofilm S. aureus and penetration depth

The membrane integrity of the biofilm *S. aureus* after plasma treatment was investigated by CLSM (Zeiss LSM710, Carl Zeiss, Jena, Germany) imaging and fluorescence quantification together with the LIVE/DEAD® BacLight™ bacterial viability kit (L7012, Molecular Probes, Carlsbad, USA) according to the manufacturer's instruction. The bacterial viability kit consisted of two types of nucleic acid dyes: SYTO 9 (green fluorescence, labeling bacteria with intact membrane structure) and PI (propidium iodide, red fluorescence, tracing membrane-damaged bacteria), which are widely used in evaluating the plasma inactivation effects by successfully

dyeing biofilm layers [32, 33, 51]. After plasma exposure, the dye mixture was added to the *S. aureus* biofilms followed by incubation at room temperature for 15–20 min. The residual dyes were washed away by dH_2O before CLSM imaging. The *z*-stack micrographs were taken from the center of the plasma-treated biofilms using Zeiss ZEN® 2010 suite (Carl Zeiss, Jena, Germany) at Ex/Em wavelengths of 485/530 nm for SYTO 9 and 485/630 nm for PI, respectively, at an interval of 1.500 μm.

A semi-quantitative assay was performed to evaluate the percentage of *S. aureus* with intact membrane structure after plasma treatment and the green/red fluorescence intensity ratio (Ratio$_{G/R}$) reflected the bacterial membrane integrity. The biofilm samples were re-suspended in PBS after exposure and added to a 96-well micro plate (Costar® 3792, Corning Inc., Corning, NY) in triplicates. The dye mixture was pipetted into the wells based on manufacturer's instruction. After thorough mixing, the samples were incubated in darkness for 25 min at room temperature. A standard microplate reader was utilized to monitor the green and red fluorescent signals at 485/530 nm and 485/630 nm, respectively and a linear fit was employed to calculate the percentage (%) of membrane-intact *S. aureus* in the population based on the Ratio$_{G/R}$. Notably, Ratio$_{G/R}$ from the counterstained 6th biofilm layer was obtained by CLSM imaging (*z*-stack) based on the fluorescence quantitative function in Zen® 2010 software. The percentage (%) of membrane-intact bacteria in this layer after plasma exposure was obtained.

2.9. Scanning electron microscopy (SEM)

SEM images were acquired from the plasma-treated *S. aureus* biofilms on the XL-30 SEM (FEI, Hillsboro, US) at 8000 magnification after gold-palladium coating.

2.10. Intracellular reactive oxygen species (ROS) of biofilm S. aureus

The cell-permeant fluorescent probe 2′,7′-dichlorodihydro-fluorescein diacetate (H_2DCFDA, D399, Sigma, US) was utilized to determine the intrabacterial ROS concentration in the biofilm *S. aureus*. The acetate groups of H_2DCFDA could be cleaved intracellularly by esterases and ROS oxidation resulting in conversion of non-fluorescent H_2DCFDA to highly fluorescent DCF (2′,7′-dichlorofluorescein) as the ROS indicator [60]. The *S. aureus* biofilms cultivated on microwell dishes were plasma-treated and dripped with H_2DCFDA (10 μM) until complete coverage. The biofilms were incubated in darkness for 20 min at 37 °C and the dye residues were removed by washing afterwards. CLSM coupled with Zeiss ZEN® 2010 software was utilized to acquire the biofilm *z*-stack images with an interval of 1.500 μm (Ex/Em at 488/525 nm) as well as the overall mean DCF intensity of the 6th biofilm layer for quantitative detection. The mean DCF intensity in a single membrane-intact bacterium in the 6th biofilm layer was obtained by using the overall DCF intensity of this layer divided by the number of membrane-intact bacteria in this layer after plasma exposure.
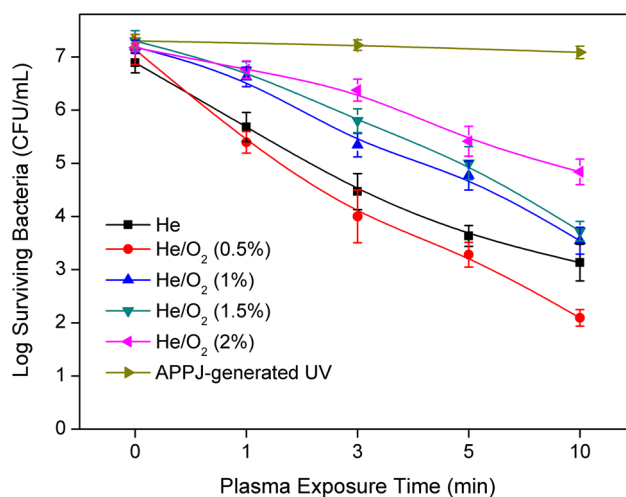

Figure 2. Log survival data of the He and He/O$_2$ APPJ treated *S. aureus* biofilms at different O$_2$ admixture ratio (0.5%–2%). Each point represents the mean of 9 values $\pm$ SD (standard deviation).

2.11. Statistical analysis

The microbiological and biochemical analyses were performed in 3 independent assays and the CFU counting results were converted to log 10 CFU ml^{-1}. The mean values and standard deviations (SD) were calculated from at least 9 measurements. The error bar represented the SD of each mean value and the significant level was assessed by the Student's T-test (SPSS V. 22.0 software).

3. Results and discussion

3.1. Surviving data of biofilm S. aureus

The deactivation efficacy of the He/O$_2$ APPJ for different O$_2$ ratios (0%, 0.5%, 1%, 1.5% and 2%) against *S. aureus* biofilms is determined. The survival data in figure 2 show that the original *S. aureus* population is approximately 7 log10 CFU ml^{-1} (different bars at $T = 0$ reflecting little variations in the initial bacteria count) and UV generated by the plasma reveals no significant disinfection effect. The inactivation effects of pure helium discharge and He/O$_2$ (0.5%) APPJ on *S. aureus* biofilms are larger than those of He/O$_2$ plasmas with higher O$_2$ admixture ratios (1%, 1.5%, and 2%) for almost all plasma exposure periods (from 0 to 10 min). Notably, the He/O$_2$ (0.5%) plasma results in a shorter *D*-value of 36 s than He APPJ (52 s) and a more than 5 log10 CFU ml^{-1} reduction (>99.999%) is obtained after He/O$_2$ plasma exposure for 10 min. More O$_2$ added ($\geqslant$1%) to helium attenuates the antimicrobial effects. The least efficient deactivation is observed at an O$_2$ ratio of 2%. Since the optimal inactivation effect is achieved with an O$_2$ ratio of 0.5%, this ratio is consequently chosen in subsequent experiments for evaluating the role of O$_2$ in He/O$_2$ plasma driven deactivation and obtaining related mehcanisms.

3.2. Characteristics of the atmospheric-pressure plasma jet

The plasma parameters such as the plasma-generated excited reactive species and gas temperature are usually determined

J. Phys. D: Appl. Phys. **50** (2017) 105201

Z Xu *et al*

by optical emission spectroscopy (OES). The OES result (200–1050 nm) of the He/O$_2$ (0.5%) plasma jet in figure 3(a) shows multi-emission lines of helium, multi-types of nitrogen species, excited OH (306–310 nm), as well as excited atomic oxygen (777.2 and 844.6 nm).

The gas temperature of the APPJ plays an important role in bacteria deactivation. Assuming that it is equal to T_{rot} (the rotational temperature), the gas temperature can be determined by comparing the simulated results in the 368–381 nm N$_2$ (C–B) band (blue dots in figure 3(b)) with the experimental results and searching for a good fit with suitable T_{rot} and T_{vib} (the vibrational temperature) in the Specair software [61]. Simulation results on T_{rot} and T_{vib} for the He and He/O$_2$ (0.5%) APPJ are supplied in figure 3(b) to display their respective evolution. As shown, a good fit is obtained at $T_{rot} = 300$ K and $T_{vib} = 2500$ K for the pure helium discharge and 310 K (T_{rot})/5000 K (T_{vib}) for the He/O$_2$ plasma. The T_{vib} significantly increases by about 2500 K when the concentration of O$_2$ goes up from 0% to 0.5% and there exists an enhancement of 10 K for the T_{rot}. More effective energy transfer from electrons to molecular oxygen through excitation of rotational and vibrational levels of O$_2$ [62] may explain the heating effect. The accuracy of the simulations is verified by monitoring the surface temperature of an APPJ-treated PTFE slice (10 min, distance at 10 mm) using an infrared thermometer (Raynger ST, Raytek, US). The two simulated T_{rot} are generally in accordance with the measured surface temperature (error of several K), respectively. Results illustrate that the gas temperature of the He and He/O$_2$ (0.5%) APPJ is close to room temperature which is also confirmed by direct contact with a human finger (figure 1). The larger T_{vib} compared to T_{rot} indicates non-equilibrium conditions suggesting highly reactive chemistry. Specifically, the near-room temperature APPJ excludes the thermo-triggered antimicrobial effects and the charged particles and reactive radicals formed in the plasma may play more critical roles in bacterial deactivation.

ROS (O and OH, etc) produce cell damage and functional perturbation by oxidation as previously reported [48, 63]. Figure 3(c) displays the line intensities of three representative plasma-generated excited ROS (309 nm ·OH, 777.2 nm O and 844.6 nm O) in the He and He/O$_2$ (0.5%) APPJ. The emission intensity of the excited hydroxyl radical (·OH, 309 nm) descreases with an admixture of O$_2$ and the excited atomic oxygen intensity (O, 777.2 nm and 844.6 nm) increases. The larger concentration of discharge-generated excited atomic O may produce better antimicrobial effects [53].

According to the OES, there are visible bands of the NO-gamma system which indicate UV radiation. UV is known to have bactericidal effect but although the APPJ source emits UV during operation, the result shows that UV-driven antimicrobial effects do not contribute much to the observed sterilization in this study (figure 2). Laroussi *et al* [64] and Machala *et al* [47] have reported that UV does not play a dominant role in plasma driven disinfection but rather the oxidizing agents are the main contributors in atmospheric-pressure plasmas composed of O$_2$ and noble gases or N$_2$.

The positive and negative ions impinging into the biofilms may produce liquid chemistry due to the biofilm encased
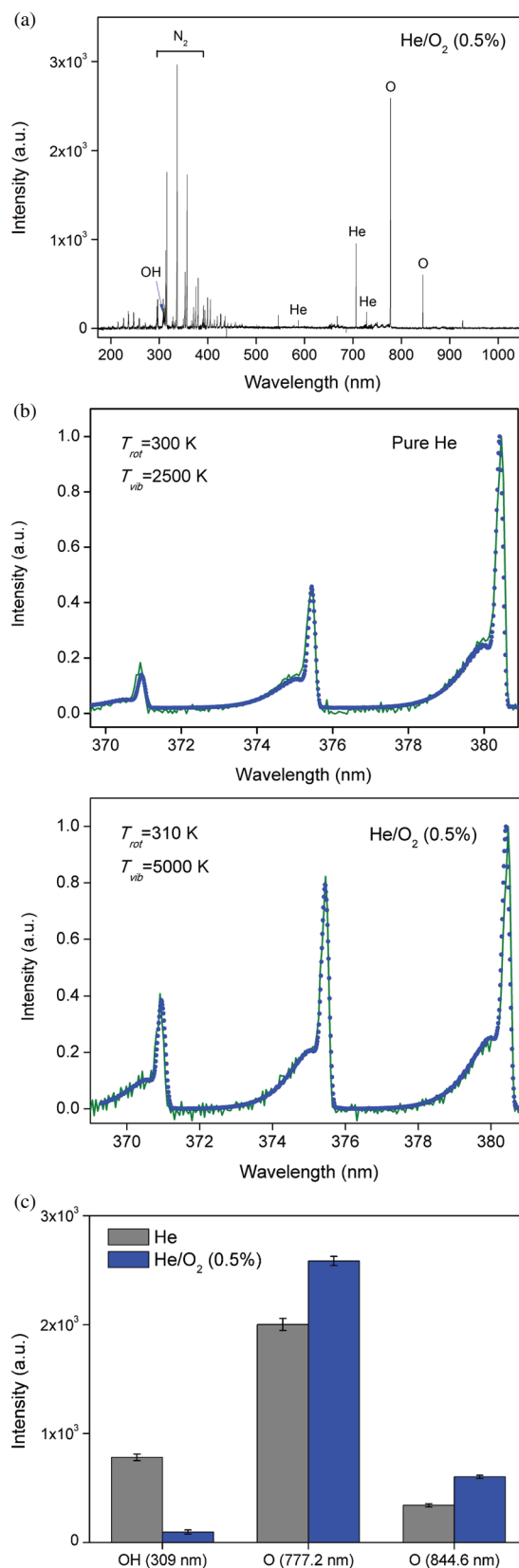

Figure 3. (a) Optical emission spectrum (OES) in the range of 200–1050 nm acquired at a distance of 10 mm below the nozzle of the He/O$_2$ (0.5%) plasma jet; (b) experimental and simulated spectra (368–381 nm) of the He and He/O$_2$ (0.5%) plasma jet; (c) emission intensities of multiple types of representative reactive species (·OH 309 nm, O 777.2 nm and O 844.6 nm) in the He and He/O$_2$ (0.5%) APPJ. Each point represents the mean of 9 values ± SD (standard deviation).
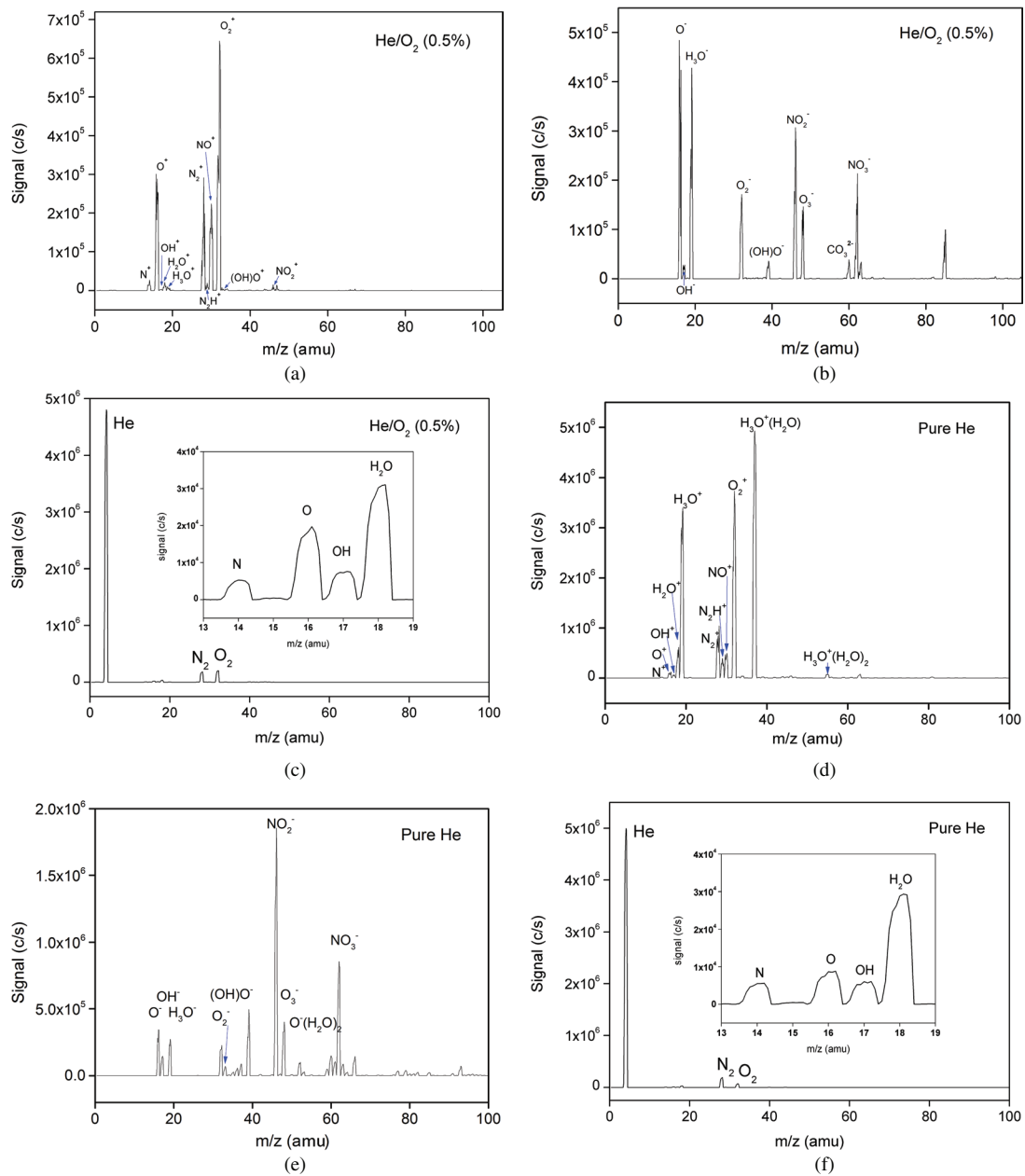
Figure 4. (a) Positive mass spectrum of He/O_2 (0.5%) APPJ; (b) negative mass spectrum of He/O_2 (0.5%) APPJ; (c) neutral mass spectrum of He/O_2 (0.5%) APPJ; (d) positive mass spectrum of He APPJ; (e) negative mass spectrum of He APPJ; (f) neutral mass spectrum of He APPJ. All mass spectra were acquired at a distance of 10 mm below the nozzle of the plasma jet.

structure and/or free H_2O. Oxidative radicals are generated and the acidity of plasma-treated zone increases leading to bacteria death [65]. Figures 4(a)–(f) present the mass spectra obtained at a distance of 10 mm from the jet nozzle. Figure 4(a) displays the positive mass spectrum of the He/O_2 (0.5%) APPJ. Nearly 20 fragments were observed such as intense peaks corresponding to O_2^+, NO^+, O^+, and N_2^+ ions as well as less intense peaks that belong to N^+, H_2O^+, H_3O^+, OH^+, (OH)O^+, N_2H^+ and NO_2^+ ions. Compared to the results obtained from the He APPJ (figure 4(d)), the O^+ intensity increases but that of OH^+ and O_2^+ decreases. The O_2^+ intensity is the highest among all positive ions in the APPJ with the admixture of O_2. Figures 4(b) and (e) show the negative mass spectra for both gases revealing more than 10 species including O^-, O_2^-, O_3^-,

OH^-, (OH)O^-, H_3O^-, CO_3^{2-}, NO_2^-, $ONOO^-$, and NO_3^-. The added O_2 increases the O^- intensity which is the largest. The intensity of O_2^- increases slightly while that of OH^- and O_3^- decreases. With regard to neutral species (figures 4(c) and (f)), He, N_2 and O_2 dominate and there are also small amounts of N, O, OH, and H_2O. In comparison, the admixture of O_2 increases the neutral O intensity. The intensity of neutral OH also increases but no appreciably.

As shown in the optical emission and mass spectra, the intensities of the excited atomic O, some O related ions and neutral O species significantly increase in the He/O_2 (0.5%) APPJ, respectively. The larger amounts of various types of ROS (reactive oxygen species) may induce stronger oxidation and destruction of the organic constituents (EPS and cell

structures) encased in the microbial biofilms giving rise to the higher antimicrobial efficacy by the He/O$_2$ (0.5%) plasma than pure helium discharge. The respective contribution of plasma generated multi-kinds of ROS on deactivation of *S. aureus* biofilms still needs further study.

3.3. Bacterial metabolic capacity of biofilm S. aureus

Irreversible conversion of resazurin to resorufin is proportional to the number of metabolically active and viable cells in the bacteria population. As shown in figure 5, the percentage of biofilm *S. aureus* with metabolic capacity decreases considerably after the He/O$_2$ (0.5%) APPJ treatment. After exposure for 10 min, it drops to approximtately 5% and the He/O$_2$ APPJ produces better inactivation effects than pure helium discharge concerning the culturable ability and metabolic capacity of biofilm *S. aureus*. By comparing figures 2 and 5, a sub-lethal effect is produced by plasma exposure bringing 5% of the biofilm *S. aureus* to a physiologically viable but non-culturable (VBNC) state [10, 66]. The transition prevents normal bacteria activities such as growth and cell division [67]. APPJ-driven environmental stresses such as energy flow, UV irradiation, toxic chemicals and water shortage limitation [68] should lead the biofilm bacteria to the VBNC state.

3.4. Bacterial membrane integrity of biofilm S. aureus

As shown in figures 6(a) and (b), the SYTO 9/PI counter-stained CLSM micrographs of He/O$_2$ (0.5%) and He APPJ treated *S. aureus* biofilms are displayed at larger intervals on plasma exposure dose (control, 5 and 10 min) and biofilm layer depth (surface, middle, bottom layer). The overwhelming majority of the biofilm *S. aureus* in all the biofilm layers at different depths are stained green after the gas treatment without discharge (serving as control) indicating good membrane integrity. After He/O$_2$ (0.5%) APPJ exposure for 5 min (figure 6(a)), the surface layer is dyed completely red signifying broken membranes on almost all bacteria. The membrane-damaged bacteria constitute a large proportion in the middle layer and are also spotted in the bottom layer. After exposure for 10 min, the layers in the *S. aureus* biofilm are predominantly stained red indicating that the plasma penetrates through all the biofilm and only a small number of membrane-intact bacteria are discernable in the bottom layer. With regard to the helium APPJ treatment (figure 6(b)), the membrane-intact bacteria still exist on the surface layer after exposure for 5 min and spotted after 10 min. For *S. aureus* in the middle layer, intact ones account for the major bacteria proportion after exposure for 5 min and it is opposite from that after 10 min. Helium plasma treatment for 10 min cannot much affect the membrane integrity of *S. aureus* in the bottom layer.

The plasma-generated ROS penetrates the biofilms layer-by-layer leading to membrane rupture on a large number of the bacteria. Penetration of the plasma into biofilms is important in elucidating the plasma-driven inactivation effect. The plasma penetration depths are obtained by method of SYTO 9/PI staining coupled with CLSM imaging (*z*-stack). The
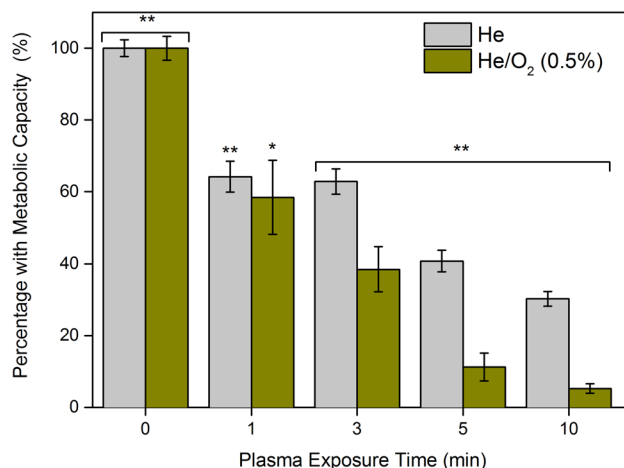

Figure 5. Percentage of bacteria with metabolic capacity in the He and He/O$_2$ (0.5%) APPJ treated *S. aureus* biofilms. Each point represents the mean of 9 values ±SD (standard deviation); significant level: $^*P < 0.05$; $^{**}P < 0.01$.

results are derived from the original CLSM *z*-stack images (data not shown). As shown in figure 7, the plasma penetration depth increases with plasma dose for both plasmas. The He plasma shows penetration depths of 0 μm (control), 12.4 μm (5 min), and 15.0 μm (10 min) and the He/O$_2$ plasma shows deeper penetration of 0 μm (control), 15.0 μm (5 min), and 16.5 μm (10 min) which has reached the bottom layer in the biofilm. Notably, the maximum penetration depth for the He/O$_2$ plasma (10 min) could be even larger with regard of the limited thickness of the cultured *S. aureus* biofilms in this study.

The He/O$_2$ (0.5%) APPJ produces better antimicrobial effects against *S. aureus* biofilms than the pure helium discharge for the same plasma dose. Figure 8 shows the percentage of membrane-intact biofilm *S. aureus* after He and He/O$_2$ (0.5%) APPJ exposure. A larger degree of membrane damage is produced by the He/O$_2$ APPJ. Prior to exposure, about 90% of the biofilm bacteria possess the intact membrane structure. After plasma exposure for 5 min, about 85% (for He/O$_2$ (0.5%) APPJ) of the bacteria population show membrane damage but only 35% after He plasma treatment. The percentages of membrane-intact bacteria decline to approximately 6% (He/O$_2$ (0.5%) APPJ) and 30% (He APPJ) after 10 min. This plasma driven anti-biofilm result is in accordance with those obtained by CFU counting (for cultivable ability) and Resazurin-based test (for metabolic capacity) in sections 3.1 and 3.3. As the electron transport chain which powers most cellular bio-physical/chemical reactions is located in the bacterial inner membrane [69], the biofilm *S. aureus* might lose the metabolic and cultivable capacity when the cellular membrane structure is damaged.

3.5. Surface morphology of S. aureus biofilms

SEM (Scanning electron microscopy) images in figure 9(a) show that the total amount of EPS (extracellular polymeric substances) decreases significantly after He and He/O$_2$ plasma exposure. In the microbial biofilms, since close to 90% of the main EPS components are organic species such as polysaccharides, proteins, and eDNAs [1], the discharge-induced
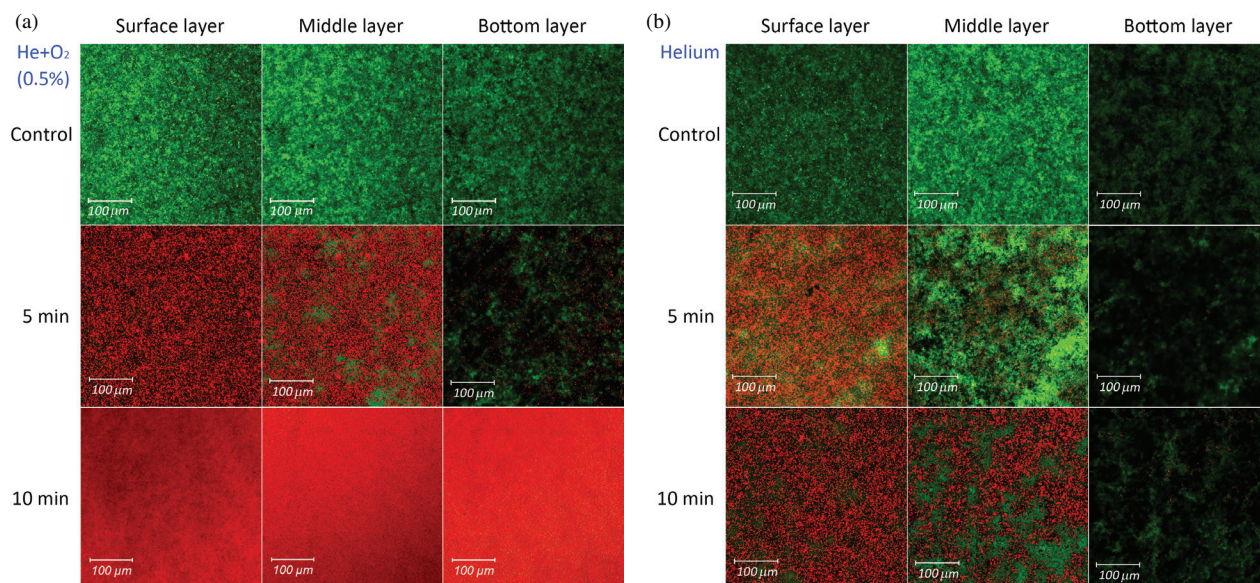
Figure 6. (a) The SYTO 9/PI stained CLSM images on bacterial membrane integrity of the He/O$_2$ (0.5%) APPJ treated *S. aureus* biofilms for different plasma dose and biofilm layers; (b) the SYTO 9/PI stained CLSM images on bacterial membrane integrity of the He APPJ treated *S. aureus* biofilms for different plasma dose and biofilm layers.
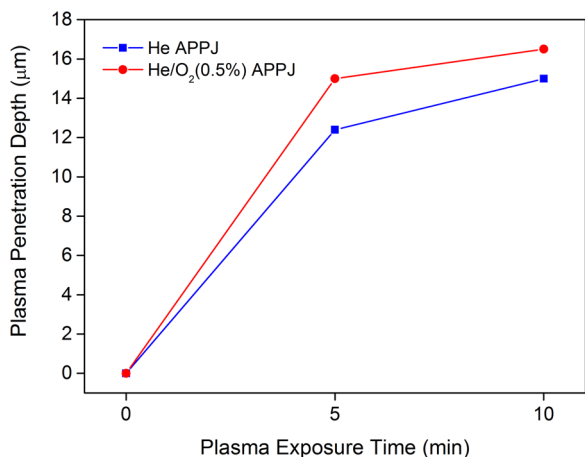

Figure 7. Penetration depth of He and He/O$_2$ (0.5%) APPJ into *S. aureus* biofilms.
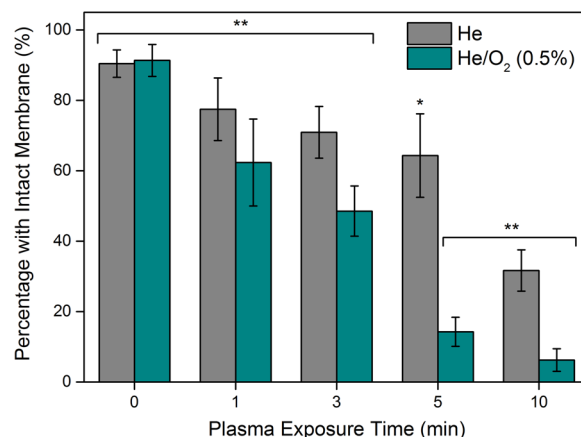

Figure 8. Percentage of bacteria with intact membrane structure in the He and He/O$_2$ (0.5%) APPJ treated *S. aureus* biofilms. Each point represents the mean of 9 values ±SD (standard deviation); significant level: $^*P < 0.05$; $^{**}P < 0.01$.

reactive species would interact with them initially, leading to attenuation of the intercellular junctions/connections among the bacteria and dispersion of cell clusters, and resulting in final impact on the inner bacteria. The shading effect derived from EPS may protect the biofilm bacteria from the plasma-driven environmental stress to some extent.

A large amount of the top-layer *S. aureus* loses the original shape, while some bacteria become smaller being a typical characteristic of VBNC bacteria [67]. Statistical analysis is performed on the diameter of a large number of bacteria ($n = 30$) in each micrograph by the Nanomeasure 2.0 software. The average diameter of the surface biofilm *S. aureus* decreases gradually with plasma dose (figure 9(b)). The He/O$_2$ (0.5%) APPJ shows larger impact on deforming the cell shape than the pure helium discharge for the same exposure time, from 0.91 μm (control) to 0.71 μm (5 min) and 0.66 μm (10 min) compared to 0.90 μm (control) to 0.77 μm (5 min) to 0.69 μm (10 min) for the helium APPJ.

The intracellular environmental stress response protects *S. aureus* by stimulating generation and secretion of various types of proteins to eliminate stress-driven side effects [70–72]. However, as the plasma dose is increased, the bacterial self-protection system is overloaded. Owing to the consequent damage, morphologically unchanged bacteria are rarely spotted from the surface biofilm layer. The reactive plasma species impinging onto the cellular structures of *S. aureus* break chemical bonds especially hydrocarbon ones, producing volatile compounds and molecular fragments [21, 73]. The plasma-driven etching effect on the bacterial outer structure may also contribute to the observed morphological change [5, 74].

Removal of the *S. aureus* biofilms is not clearly observed from the SEM photos after He/O$_2$ (0.5%) and He APPJ exposure in this study. In comparison, Idlibi *et al* [75] found removal of the oral biofilm by a cold atmospheric-pressure plasma
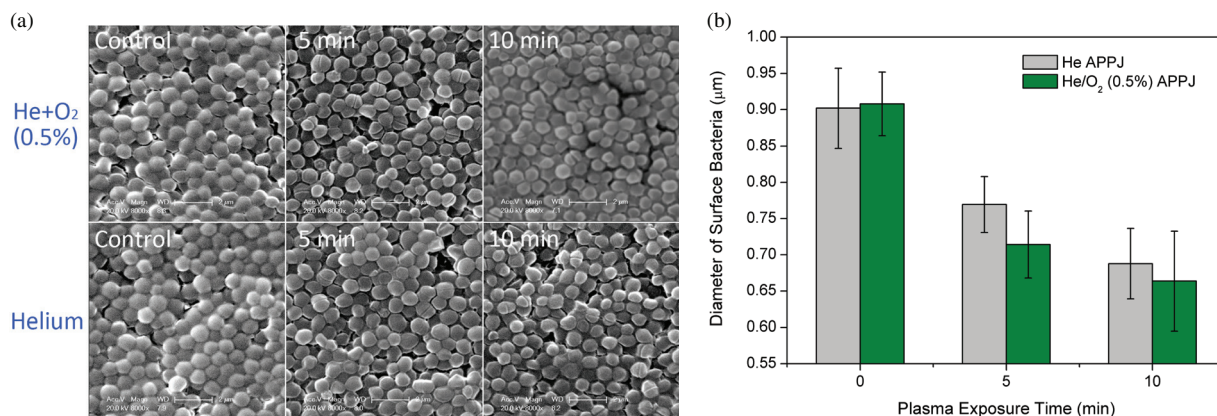
J. Phys. D: Appl. Phys. **50** (2017) 105201

Z Xu *et al*

Figure 9. SEM micrographs of the He and He/O$_2$ (0.5%) APPJ treated *S. aureus* biofilms; (b) average diameter of *S. aureus* in the surface biofilm layer after He and He/O$_2$ (0.5%) APPJ exposure.
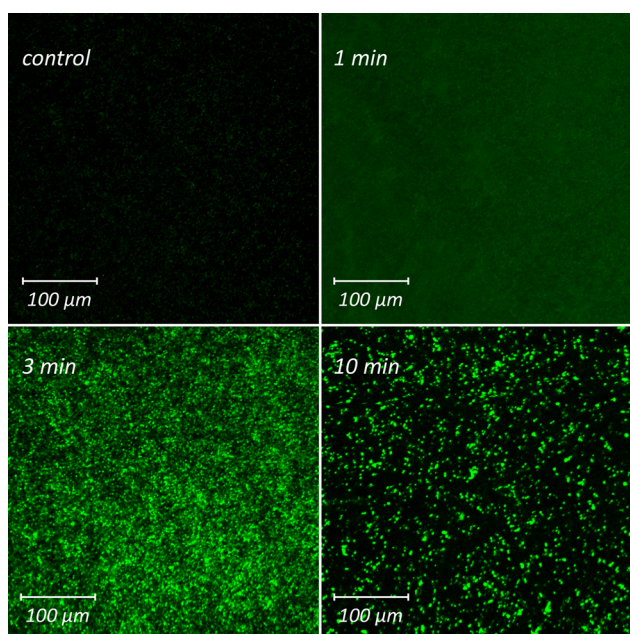

Figure 10. H$_2$DCFDA stained CLSM images acquired from the 6th layer of the He/O$_2$ (0.5%) APPJ treated *S. aureus* biofilms. The highly fluorescent DCF serves as an indicator for intracellular ROS.

Figure 11. Overall mean DCF fluorescence intensity (RFU μm^{-2}, at Ex/Em: 488/525 nm) of the 6th biofilm layer and the mean DCF intensity within a single membrane intact *S. aureus* located in the 6th biofilm layer after He/O$_2$ (0.5%) APPJ treatment. The highly fluorescent DCF serves as an indicator for intracellular ROS. Each point represents the mean of 9 values $\pm$ SD (standard deviation); significant level: $^{**}P < 0.01$.

3.6. Intracellular ROS of biofilm S. aureus

The intrabacterial ROS status of biofilm *S. aureus* is investigated to elucidate their effects in the plasma-driven inactivation process as well as related mechanism and to establish the relationship between cell death and intracellular ROS concentrations. Figure 10 displays the H$_2$DCFDA stained CLSM micro-images acquired from the 6th biofilm layer immediately after He/O$_2$ (0.5%) APPJ exposure. The continuously diminishing green dots imply that more and more *S. aureus* in this layer suffer from membrane damage, as the fluorescence probe cannot be encased but instead leaked and washed away from the membrane-damaged cells. However, the intensity of green fluorescence emitted from each intact cell increases,
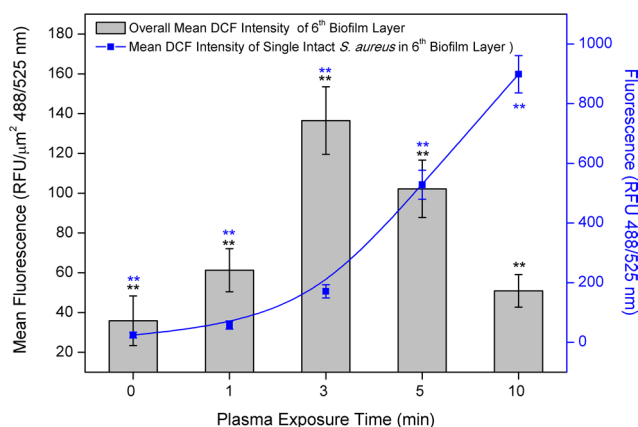
albeit not always completely. Rupf *et al* [76] observed total removal of biofilms using an Ar–O$_2$ plasma in combination with air/water spray (mechanical cleaning).

indicating that the intracellular ROS concentration in each membrane-intact bacterium in this layer increases during exposure before its membrane is finally damaged.

As shown in figure 11, the overall mean DCF intensity of the 6th biofilm layer does not change appreciably but only exhibits a small up-and-down tendency. It denotes the overall mean intracellular ROS concentration in each μm^2 of this layer derived from membrane-intact *S. aureus* after the plasma treatment. Plasma exposure produces different environmental stress including reactive species, electric field, UV radiation, etc. The stress, especially RS attack, can damage the external cellular structure by oxidation and disrupt the balance in the intrabacterial ROS concentrations through penetration, subsequently inducing intracellular self-protection responses as signal molecules [77]. Specified 'defending genes' are thus stimulated in generating and secreting multiple kinds of proteins to repair cellular damage [71, 72]. However, in the shielding processes, more ROS such as $\cdot$O$_2^-$, $\cdot$OH, ^{1}O$_2$, and H$_2$O$_2$ are generated as by-products by the bacterial metabolic systems [69, 77]. Therefore, to resist the impact originating from the penetration of plasma-generated ROS and

J. Phys. D: Appl. Phys. **50** (2017) 105201

Z Xu *et al*

plasma-induced endogenous ROS, the bacterial oxidative stress response system keeps working to maintain an intrinsic balance state of intracellular ROS at a relatively stable level via different bacterial metabolic pathways [69]. It is the primary reason for the initially mild enhancement of the overall mean DCF intensity in the 6th biofilm layer. As the exposure dose is increased, the threshold of the bacterial self-protection capacity is exceeded as described in section 3.5. Beyond the intrinsic threshold of ROS elimination in *S. aureus* after high-dose plasma exposure, the intracellular ROS with strong reactive potency impact the bacterial membrane inside in concert with the plasma-generated ROS from the outside, causing heavy damage to bacterial structure and mediated functions. Therefore, an increasing number of biofilm *S. aureus* shows damaged membranes (figure 8). The DCF probes leak and are washed away from the membrane-damaged cells decreasing the overall mean DCF intensity of this layer.

The decrease is still moderate after He/O$_2$ (0.5%) APPJ treatment for 10 min even the membrane structure of a large amount of bacteria in this layer is damaged under these conditions. That is because the intracellular ROS concentration in each membrane-intact *S. aureus* in the 6th biofilm layer continues to increase, averagely harboring a high level of DCF (signifying intracellular ROS concentrations) at about 900 RFU (relative fluorescence units). It is more than 36 times compared with the untreated bacteria (control) in the same layer (figure 11). The results show a selection of specially ROS adapted bacteria located in deeper layers (such as 6th) of the biofilm. Considering the predominance of the reactive oxidative species (ROS) driven antimicrobial effects, it is rather difficult to eradicate microbial biofilms using plasma techniques solely. Owing to the high resistance of microbial biofilms to antibiotics, other methods such as mechanical cleaning [76] should be combined to achieve a potentially optimal antimicrobial efficacy in practical applications.

4. Conclusion

The inactivation effects and mechanism on *S. aureus* biofilms by a He/O$_2$ APPJ are investigated. Mixture of O$_2$ (0.5%) in helium generates a larger amount of reactive oxygen species to deactivate the biofilm bacteria. More than 5 log10 ml^{-1} CFU reduction is observed after He/O$_2$ (0.5%) APPJ treatment for 10 min and it is the optimal antimicrobial effect. Meanwhile, 95% of the total biofilm *S. aureus* population lose the metabolic capacity and the remaining 5% may enter the sub-lethal viable but non-culturable (VBNC) state for self-protection. With this plasma dose, the He/O$_2$ (0.5%) APPJ can penetrate through all the biofilm layers producing damage in the bacterial membranes. A larger penetration depth into the *S. aureus* biofilms is observed for the He/O$_2$ (0.5%) APPJ than for the helium discharge at the same plasma dose. SEM reveals that the plasma erodes the EPS first and then the cellular structure, deforming the bacterial shape and the *S. aureus* in the surface layer possess a smaller average diameter after He/O$_2$ (0.5%) plasma treatment. The rising intracellular ROS concentrations play a pivotal role in damaging the bacterial

membrane structure during exposure. The ROS generated by the APPJ and plasma-induced endogenous ROS may attack the bacterial membrane structure from the outside and inside to produce heavy damage in the structures and mediated functions synergistically. The inactivated biofilm *S. aureus* are still attached to the colonizing surface and the biofilm thickness does not decrease obviously according to SEM and CLSM micrographs, indicating no significant removal of the *S. aureus* biofilms by the He and He/O$_2$ (0.5%) APPJ.

References

[1] Costerton J, Stewart P and Greenberg E 1999 Bacterial biofilms: a common cause of persistent infections *Science* **284** 1318–22
[2] Donlan R and Costerton J 2002 Biofilms: survival mechanisms of clinically relevant microorganisms *Clin. Microbiol. Rev.* **15** 167–93
[3] Fey P D 2010 Modality of bacterial growth presents unique targets: how do we treat biofilm-mediated infections? *Curr. Opin. Microbiol.* **13** 610–5
[4] Hueso J L, Rico V J, Fras J E, Cotrino J and Gonzlezelipe A R 2008 Ar + NO microwave plasmas for *Escherichia coli* sterilization *J. Phys. D: Appl. Phys.* **41** 092002
[5] Shen J *et al* 2014 Observation of inactivation of *Bacillus subtilis* spores under exposures of oxygen added argon atmospheric pressure plasma jet *Japan. J. Appl. Phys.* **53** 110310
[6] Goree J, Liu B and Drake D 2006 Gas flow dependence for plasma-needle disinfection of *S. mutans* bacteria *J. Phys. D: Appl. Phys.* **39** 3479–86
[7] Cheng C, Shen J, Xiao D Z, Xie H B, Lan Y, Fang S D, Meng Y D and Chu P K 2014 Atmospheric pressure plasma jet utilizing Ar and Ar/H$_2$O mixtures and applications to bacteria inactivation *Chin. Phys.* B **23** 075204
[8] Kovalóvá Z, Zahoran M, Zahoranová A and Machala Z 2014 *Streptococci* biofilm decontamination on teeth by low-temperature air plasma of DC corona discharges *J. Phys. D: Appl. Phys.* **47** 224014
[9] Shen J *et al* 2015 Characteristics of DC gas–liquid phase atmospheric-pressure plasma and bacteria inactivation mechanism *Plasma Process. Polym.* **12** 252–9
[10] Marchal F *et al* 2012 Inactivation of gram-positive biofilms by low-temperature plasma jet at atmospheric pressure *J. Phys. D: Appl. Phys.* **45** 345202
[11] Xiao D Z, Cheng C, Lan Y, Ni G H, Shen J, Meng Y D and Chu P K 2016 Effects of atmospheric-pressure non-thermal nitrogen and air plasma on bacteria inactivation *IEEE Trans. Plasma Sci.* **44** 2699–707
[12] Ermolaeva S A, Sysolyatina E V and Gintsburg A L 2015 Atmospheric pressure nonthermal plasmas for bacterial biofilm prevention and eradication *Biointerphases* **10** 029404

J. Phys. D: Appl. Phys. **50** (2017) 105201

Z Xu *et al*

[13] Woedtke T V, Reuter S, Masur K and Weltmann K D 2013 Plasmas for medicine *Phys. Rep.* **530** 291–320

[14] Scholtz V, Pazlarová J, Soušková H, Khun J and Julák J 2015 Nonthermal plasma-a tool for decontamination and disinfection *Biotechnol. Adv.* **33** 1108–19

[15] O'Connor N, Cahill O, Daniels S, Galvin S and Humphreys H 2014 Cold atmospheric pressure plasma and decontamination. Can it contribute to preventing hospital-acquired infections? *J. Hosp. Infect.* **88** 59–65

[16] Yousfi M, Merbahi N, Pathak A and Eichwald O 2014 Low-temperature plasmas at atmospheric pressure: toward new pharmaceutical treatments in medicine *Fundam. Clin. Pharmacol.* **28** 123–35

[17] Halfmann H, Bibinov N, Wunderlich J and Awakowicz P 2007 A double inductively coupled plasma for sterilization of medical devices *J. Phys. D: Appl. Phys.* **40** 4145–54

[18] Joaquin J C, Kwan C, Abramzon N, Vandervoort K and Brelles-Mariño G 2009 Is gas-discharge plasma a new solution to the old problem of biofilm inactivation? *Microbiol.* **155** 724–32

[19] Ehlbeck J *et al* 2011 Low temperature atmospheric pressure plasma sources for microbial decontamination *J. Phys. D: Appl. Phys.* **44** 013002

[20] Matthes R *et al* 2013 Antimicrobial efficacy of two surface barrier discharges with air plasma against *in vitro* biofilms *PloS One* **8** e70462

[21] Fricke K *et al* 2012 Atmospheric pressure plasma: a high-performance tool for the efficient removal of biofilms *PloS One* **7** e42539

[22] Alkawareek M Y *et al* 2012 Application of atmospheric pressure non-thermal plasma for the *in vitro*, eradication of bacterial biofilms *FEMS Immunol. Med. Microbiol.* **65** 381–4

[23] Delben J A *et al* 2016 Effect of atmospheric-pressure cold plasma on pathogenic oral biofilms and *in vitro* reconstituted oral epithelium *PloS One* **11** e0155427

[24] Taghizadeh L *et al* 2015 Inactivation of biofilms using a low power atmospheric pressure argon plasma jet; the role of entrained nitrogen *Plasma Process. Polym.* **12** 75–81

[25] Matthes R, Assadian O and Kramer A 2014 Repeated applications of cold atmospheric pressure plasma does not induce resistance in *Staphylococcus aureus* embedded in biofilms *GMS Hyg. Infect. Control* **9** Doc17

[26] Matthes R *et al* 2013 Antimicrobial efficacy of an atmospheric pressure plasma jet against biofilms of *Pseudomonas aeruginosa*, and *Staphylococcus epidermidis Plasma Process. Polym.* **10** 161–6

[27] Alkawareek M Y *et al* 2012 Eradication of *Pseudomonas aeruginosa* biofilms by atmospheric pressure non-thermal plasma *PloS One* **7** e44289

[28] Rupf S *et al* 2010 Killing of adherent oral microbes by a non-thermal atmospheric plasma jet *J. Med. Microbiol.* **59** 206–12

[29] Gorynia S *et al* 2013 *In vitro* efficacy of cold atmospheric pressure plasma on *S. sanguinis* biofilms in comparison of two test models GMS *Hyg. Infect. Control* **8** Doc01

[30] Koban I *et al* 2010 Treatment of *Candida albicans* biofilms with low-temperature plasma induced by dielectric barrier discharge and atmospheric pressure plasma jet *New J. Phys.* **12** 073039

[31] Koban I *et al* 2011 Antimicrobial efficacy of non-thermal plasma in comparison to chlorhexidine against dental biofilms on titanium discs *in vitro*-proof of principle experiment *J. Clin. Periodontol.* **38** 956–65

[32] Xiong Z, Du T, Lu X, Cao Y and Pan Y 2011 How deep can plasma penetrate into a biofilm? *Appl. Phys. Lett.* **98** 221503

[33] Pei X *et al* 2012 Inactivation of a 25.5 μm *Enterococcus faecalis* biofilm by a room-temperature, battery-operated, handheld air plasma jet *J. Phys. D: Appl. Phys.* **45** 165205

[34] Sysoliatina E V *et al* 2013 Bactericidal action of non-thermal plasma on biofilms formed *in vitro* and within a root channel *Zh. Mikrobiol. Epidemiol. Immunobiol.* **6** 8–12

[35] Vandervoort K G and Brelles-Mariño G 2014 Plasma-mediated inactivation of *Pseudomonas aeruginosa* biofilms grown on borosilicate surfaces under continuous culture system *PLoS One* **9** e108512

[36] Zelaya H, Haro C, Laiño J, Alvarez S and Agüero G 2011 Coagulation activation in an experimental pneumonia model in malnourished mice *Can. J. Physiol. Pharmacol.* **89** 41–9

[37] Flynn P B *et al* 2015 Bactericidal efficacy of atmospheric pressure non-thermal plasma (APNTP) against the ESKAPE pathogens *Int. J. Antimicrob. Ag.* **46** 101–7

[38] Walsh J L, Iza F, Janson N B, Law V J and Kong M G 2010 Three distinct modes in a cold atmospheric pressure plasma jet *J. Phys. D: Appl. Phys.* **43** 075201

[39] Lu X, Naidis G V, Laroussi M and Ostrikov K 2014 Guided ionization waves: theory and experiments *Phys. Rep.* **540** 123–66

[40] Xiao D *et al* 2014 Characteristics of atmospheric-pressure non-thermal N_2 and N_2/O_2 gas mixture plasma jet *J. Appl. Phys.* **115** 033303

[41] Xiao D *et al* 2014 Electron density measurements of atmospheric-pressure non-thermal N_2 plasma jet by stark broadening and irradiance intensity methods *Phys. Plasmas* **21** 053510

[42] Yonemori S and Ono R 2014 Flux of OH and O radicals onto a surface by an atmospheric-pressure helium plasma jet measured by laser-induced fluorescence *J. Phys. D: Appl. Phys.* **47** 125401

[43] Judée F, Wattieaux G, Merbahi N, Mansour M and Castaniécornet M P 2014 The antibacterial activity of a microwave argon plasma jet at atmospheric pressure relies mainly on UV-C radiations *J. Phys. D: Appl. Phys.* **47** 405201

[44] Norberg S A, Johnsen E and Kushner M J 2016 Helium atmospheric pressure plasma jets interacting with wet cells: delivery of electric fields *J. Phys. D: Appl. Phys.* **49** 185201

[45] Stoffels E, Sakiyama Y and Grave D B 2008 Cold atmospheric plasma: charged species and their interactions with cells and tissues *IEEE Trans. Plasma Sci.* **36** 1441–57

[46] Lu X, Naidis G V, Laroussi M, Reuter S, Graves D B and Ostrikov K 2016 Reactive species in non-equilibrium atmospheric-pressure plasmas: generation, transport, and biological effects *Phys. Rep.* **630** 1–84

[47] Machala Z, Chladekova L and Pelach M 2010 Plasma agents in bio-decontamination by DC discharges in atmospheric air *J. Phys. D: Appl. Phys.* **43** 222001

[48] Graves D B 2012 The emerging role of reactive oxygen and nitrogen species in redox biology and some implications for plasma applications to medicine and biology *J. Phys. D: Appl. Phys.* **45** 263001

[49] Zhang H *et al* 2015 Effects and mechanism of atmospheric-pressure dielectric barrier discharge cold plasma on lactate dehydrogenase (LDH) enzyme *Sci. Rep.* **5** 10031

[50] Babaeva N Y and Kushner M J 2010 Intracellular electric fields produced by dielectric barrier discharge treatment of skin *J. Phys. D: Appl. Phys.* **43** 185206

[51] Xu Z *et al* 2015 Inactivation effects of non-thermal atmospheric-pressure helium plasma jet on *Staphylococcus aureus* biofilms *Plasma Process. Polym.* **12** 827–35

[52] Caplan S R and Sollner K 2008 On the application of inductively coupled plasma discharges sustained in $Ar/O_2/ N_2$ ternary mixture for sterilization and decontamination of medical instruments *J. Phys. D: Appl. Phys.* **41** 192005

[53] Shen J *et al* 2012 Sterilization of *Bacillus subtilis* spores using an atmospheric plasma jet with argon and oxygen mixture gas *Appl. Phys. Express* **5** 036201

J. Phys. D: Appl. Phys. 50 (2017) 105201

Z Xu et al

[54] Kylián O and Rossi F 2009 Sterilization and decontamination of medical instruments by low-pressure plasma discharges: application of Ar/O$_2$/N$_2$ ternary mixture *J. Phys. D: Appl. Phys.* **42** 085207

[55] Pointu A M, Ricard A, Dodet B, Odic E, Larbre J and Ganciu M 2005 Production of active species in N$_2$–O$_2$ flowing post-discharges at atmospheric pressure for sterilization *J. Phys. D: Appl. Phys.* **38** 1905–9

[56] Nguyen D B *et al* 2013 Invasive methicillin-resistant *Staphylococcus aureus* infections among patients on chronic dialysis in the united states, 2005–2011 *Clin. Infec. Dis.* **57** 1393–400

[57] Sato T, Miyahara T, Doi A, Ochiai S, Urayama T and Nakatani T 2006 Sterilization mechanism for *Escherichia coli* by plasma flow at atmospheric pressure *Appl. Phys. Lett.* **89** 073902

[58] Matthes R *et al* 2014 Efficacy of different carrier gases for barrier discharge plasma generation compared to chlorhexidine on the survival of *Pseudomonas aeruginosa* embedded in biofilm *in vitro Skin Pharmacol. Physiol.* **27** 148–57

[59] O'Brien J, Wilson I, Orton T and Pognan F 2000 Investigation of the alamar blue (resazurin) fluorescent dye for the assessment of mammalian cell cytotoxicity *Eur. J. Biochem.* **267** 5421–6

[60] Kalyanaraman B *et al* 2012 Measuring reactive oxygen and nitrogen species with fluorescent probes: challenges and limitations *Free Radical Biol. Med.* **52** 1–6

[61] Laux C O, Spence T G, Kruger C H and Zare R N 2003 Optical diagnostics of atmospheric pressure air plasmas *Plasma Sources Sci. Trans.* **12** 125–38

[62] Deng X L, Nikiforov A Y, Vanraes P and Leys C 2013 Direct current plasma jet at atmospheric pressure operating in nitrogen and air *J. Appl. Phys.* **113** 023305

[63] Liu D X, Rong M Z, Wang X H, Iza F, Kong M G and Bruggeman P 2010 Main species and physicochemical processes in cold atmospheric-pressure He + O$_2$ plasmas *Plasma Process. Polym.* **7** 846–65

[64] Laroussi M 2005 Low temperature plasma-based sterilization: overview and state-of-the-art *Plasma Process. Polym.* **2** 391–400

[65] Van Gils C A J, Hofmann S, Boekema B K H L, Brandenburg R and Bruggeman P J 2013 Mechanisms of bacterial inactivation in the liquid phase induced by a remote RF cold atmospheric pressure plasma jet *J. Phys. D: Appl. Phys.* **46** 175203

[66] Vandervoort K, Abramzon N and Brelles-Mariño G 2008 Plasma interactions with bacterial biofilms as visualized through atomic force microscopy *IEEE Trans. Plasma Sci.* **36** 1296–7

[67] Trevors J T 2011 Viable but non-culturable (VBNC) bacteria: gene expression in planktonic and biofilm cells *J. Microbiol. Methods* **86** 266–73

[68] Lleo M M, Bonato B, Tafi M C, Signoretto C, Boaretti M and Canepari P 2001 Resuscitation rate in different *Enterococcal* species in the viable but non-culturable state *J. Appl. Microbiol.* **91** 1095–102

[69] Karp G and Geer P V D 2005 *Cell and Molecular Biology* (Hoboken, NJ: Wiley)

[70] Xu Z *et al* 2015 Genetic effects of an air discharge plasma on *Staphylococcus aureus* at the gene transcription level *Appl. Phys. Lett.* **106** 213701

[71] Pomposiello P J and Demple B 2001 Redox-operated genetic switches: the soxR and oxyR transcription factors *Trends Biotechnol.* **19** 109–14

[72] Cabiscol E, Tamarit J and Ros J 2000 Oxidative stress in bacteria and protein damage by reactive oxygen species *Int. Microbiol.* **3** 3–8

[73] Pompl P *et al* 2009 The effect of low temperature plasma on bacteria as observed by repeated AFM imaging *New J. Phys.* **11** 115023

[74] Zhao Y, Ogino A and Nagatsu M 2011 Mass spectrometric study on inactivation mechanism of spore-forming bacteria by low-pressure surface-wave excited oxygen plasma *Appl. Phys. Lett.* **98** 191501

[75] Idlibi A N *et al* 2013 Destruction of oral biofilms formed *in situ* on machined titanium (Ti) surfaces by cold atmospheric plasma *Biofouling* **29** 369e379

[76] Rupf S *et al* 2011 Removing biofilms from micro-structured titanium *ex vivo*: a novel approach using atmospheric plasma technology *PloS One* **6** e25893

[77] Apel K and Hirt H 2004 Reactive oxygen species: metabolism, oxidative stress, and signal transduction *Annu. Rev. Plant Biol.* **55** 728–49